ACS POLYMERS Au
AN OPEN ACCESS JOURNAL OF THE AMERICAN CHEMICAL SOCIETY

pubs.acs.org/polymerau

Article

# Self-Reporting Polysaccharide Polymersome for Doxorubicin and Cisplatin Delivery to Live Cancer Cells

Mishika Virmani, Nilesh Umakant Deshpande, Shahidkhan Pathan, and Manickam Jayakannan*

Cite This: *ACS Polym. Au* 2022, 2, 181−193

Read Online

ACCESS | Metrics & More | Article Recommendations | Supporting Information

**ABSTRACT:** We report self-reporting fluorescent polysaccharide polymersome nanoassemblies for enzyme-responsive intracellular delivery of two clinical anticancer drugs doxorubicin (DOX) and cisplatin to study the real-time drug-releasing aspects by fluorescent resonance energy transfer (FRET) bioimaging in live cancer cells. Fluorescent polymersomes were tailor-made by tagging an aggregation-induced emission (AIE) optical chromophore, tetraphenylethylene (TPE), and a plant-based vesicular directing hydrophobic unit through enzyme-biodegradable aliphatic ester chemical linkages in the polysaccharide dextran. The blue-luminescent polymersome self-assembled in water and exhibited excellent encapsulation capability for the red-luminescent anticancer drug DOX. FRET between the AIE polymersome host and DOX guest molecules resulted in a completely turn-off probe. At the intracellular level, the lysosomal enzymatic disassembly of the polymersome restored the dual fluorescent signals from DOX and TPE at the nucleus and the lysosomes, respectively. Live-cell confocal microscopy coupled with selective photoexcitation was employed to study the real-time polymersome disassembly by monitoring the turn-on fluorescent signals in human breast cancer cell lines. Alternatively, carboxylic acid-functionalized AIE polymersomes were also tailor-made for cisplatin stitching to directly monitor Pt drug delivery. The polymersome nanoassemblies exhibited excellent structural tolerance for the chemical conjugation of the Pt drugs, and the fluorescence signals were unaltered. An in vitro drug release study confirmed that the cisplatin-stitched fluorescent polymersomes were very stable under physiological conditions and underwent lysosomal enzymatic degradation to inhibit the cancer cell growth. A lysosomal colocalization experiment using confocal microscopy substantiates the enzyme-responsive degradation of these polymersomes to release both the encapsulated and conjugated drugs at the intracellular level. The present design provides a unique opportunity to deliver more than one anticancer drug from a single polymersome platform in cancer research.

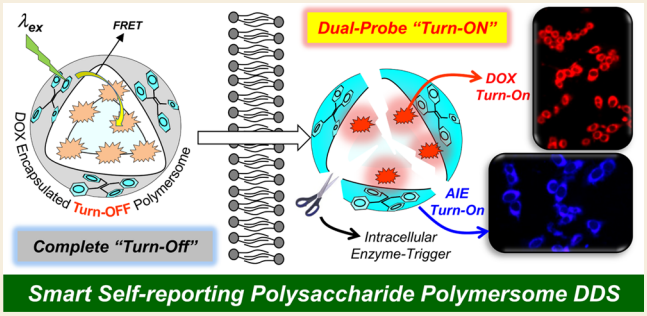


**KEYWORDS:** *drug delivery, fluorescent probes, polymersomes, enzyme-responsive, polysaccharides, cisplatin, doxorubicin*

## INTRODUCTION

Enlarging therapeutic effects of anticancer drugs has become the holy grail of oncotherapy, thereby paving the way for the development of drug-delivery systems (DDSs) in cancer treatment.[1−4] Multitudes of delivery scaffolds ranging from liposomes,[5] microspheres,[6] dendrimers,[7] polymeric drug conjugates,[8] polymeric micelles,[9] and polymersomes[10−12] have been a subject of extensive clinical research. The rationale of loading therapeutics in delivery vehicles is to reduce systemic toxicity by shielding the drug against a plethora of plasma components during its transport via the bloodstream and later accumulating inside the target site leading to enhanced efficacy.[13] The choice of the delivery scaffold and its concomitant effects on drug efficacy is worth paying attention to improve the cancer treatment.[14] For instance, liposomal encapsulation of the chemotherapy drug doxorubicin (DOX) has shown considerable reduction in cardiotoxicity, simultaneously maintaining a high level of efficacy.[15,16] Surprisingly, liposomal formulation of cisplatin-conjugated drug (SPI-77 or stealth cisplatin) showed rather poor efficacy owing to slow release inside the tumor.[17,18] The problem of reduced efficacy due to poor uptake can be mitigated by a thoughtful choice of engineering the structural aspects of the nanoscaffold. Sugars are ubiquitous to cell membranes, and hence, polysaccharide-based scaffolds such as dextran become candidates of choice as they are easily taken up by the cells owing to like−like interactions.[8,19−21] Tagging the scaffold with a fluorophore can further help shed light on its uptake mechanism at the cellular level and also enable the tracking of the polymer nanocarriers.[22,23] Therefore, next-generation polymer nanocarriers are required to create a smart self-

Received: September 30, 2021
Revised: December 11, 2021
Accepted: December 13, 2021
Published: December 28, 2021

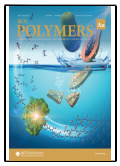





https://doi.org/10.1021/acspolymersau.1c00042
*ACS Polym. Au* 2022, 2, 181−193

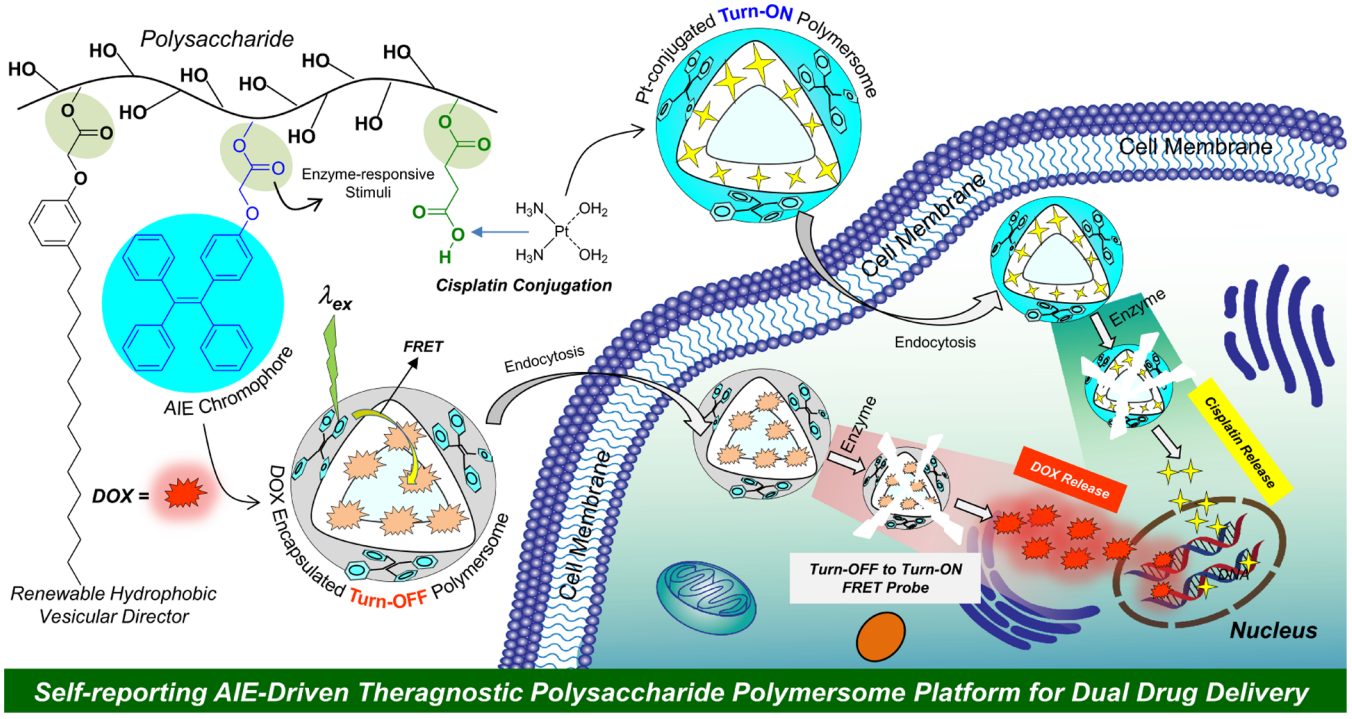


**Figure 1.** AIE-activated and enzyme-responsive fluorescent polysaccharide self-reporting polymersome platform for the dual delivery of cisplatin and DOX to cancer cells.

reporting system, while they administrate the drug molecules. DDSs employing aggregation-induced emission (AIE)gen such as tetraphenylethylene (TPE) have recently gained considerable attention in bioimaging applications.[24−27] Conventional fluorophores or dyes typically undergo aggregation-caused quenching (ACQ) owing to strong $\pi-\pi$ stacking in water, thereby limiting their usage in bioimaging applications.[28] AIEgens display fluorescence in highly aggregated states due to restriction of intramolecular rotation (RIM), thereby augmenting their usage in biological imaging.[29] The second problem of slower release kinetics inside the cells can be fine-tuned by the choice of the chemical linkages in DDSs. Employing pH-sensitive linkages such as oxime,[30] imines,[31] and acetals[32] and enzyme-sensitive linkages such as aliphatic esters[33,34] offers release in a more controlled manner. Self-reporting enzyme-responsive and AIEgen polysaccharide DDSs capable of loading a multitude of drugs with unperturbed efficacies are rather scarce in the literature. Polymersomes are important classes of DDSs due to their unique capability to load both water-soluble and -insoluble drug molecules.[1,35,36] From our research group, we have reported a renewable resource[37] approach to develop polysaccharide polymersomes for targeted and combination therapy of wide ranges of anticancer drugs.[35,38−43] AIE-based polymersomes were reported in the past for material application in $CO_2$ capture;[44,45] however, they are very rarely explored in biomedical research.[46] Hence, the development of fluorescent polysaccharide polymersomes for both chemical conjugation and encapsulation of clinically important anticancer drugs such as cisplatin and DOX in a single polymersome nanocarrier would be very important for achieving both therapeutic and bioimaging together in cancer research.

Herein, we report a polysaccharide (dextran)-based scaffold tagged with an AIE chromophore, TPE, which behaves as an excellent self-reporting nanoassembly for drug delivery as shown in Figure 1.[46] Dextran was conjugated with renewable 3-pentadecylphenol (PDP) and TPE via ester linkages and the resultant amphiphile was self-assembled into fluorescent polymersomes in water of size less than 200 nm. Uptake of polymersomes via endocytosis was very well-monitored due to its intrinsic blue luminescence via confocal microscopy. The blue-luminescent vesicles were capable of loading the anticancer drug DOX. The intact assembly encapsulating DOX underwent fluorescence quenching when excited at a TPE excitation wavelength leading to a turn-off probe which turned on inside the cells in a time-dependent manner, shedding more light on the release kinetics of this versatile DDS. Independently, the abovementioned scaffold was also modified with an acid functional handle so as to conjugate another clinically important drug cisplatin. The cisplatin-conjugated blue-luminescent vesicles showed enhanced efficacy in comparison with the free counterpart. The polymersomes conjugated with cisplatin were taken via endocytosis as confirmed via a Lysotracker experiment. This unique scaffold, irrespective of the drug loaded (such as DOX or chemically conjugated like cisplatin), was readily taken up by the cell as monitored via the emission of TPE. Luminescent polymersomes open up a multitude of opportunities in cancer research by not only preserving the drug efficacy but also simultaneously allowing the tracking of both the drug and scaffold at the cellular level by bioimaging.

## RESULTS AND DISCUSSION

### Synthesis and Self-Assembly of Polymersomes

The polysaccharide derivative DEX−PDP−TPE−COOH was synthesized by coupling PDP acid, TPE acid, and tertiary butyl ester of succinic acid (SA) to the dextran backbone in a one-pot reaction using DCC/DMAP coupling via aliphatic ester linkages, as described in Scheme 1. The deprotection of the *t*-


https://doi.org/10.1021/acspolymersau.1c00042
ACS Polym. Au 2022, 2, 181−193

**Scheme 1. Synthesis of TPE-Conjugated Dextran Derivatives**

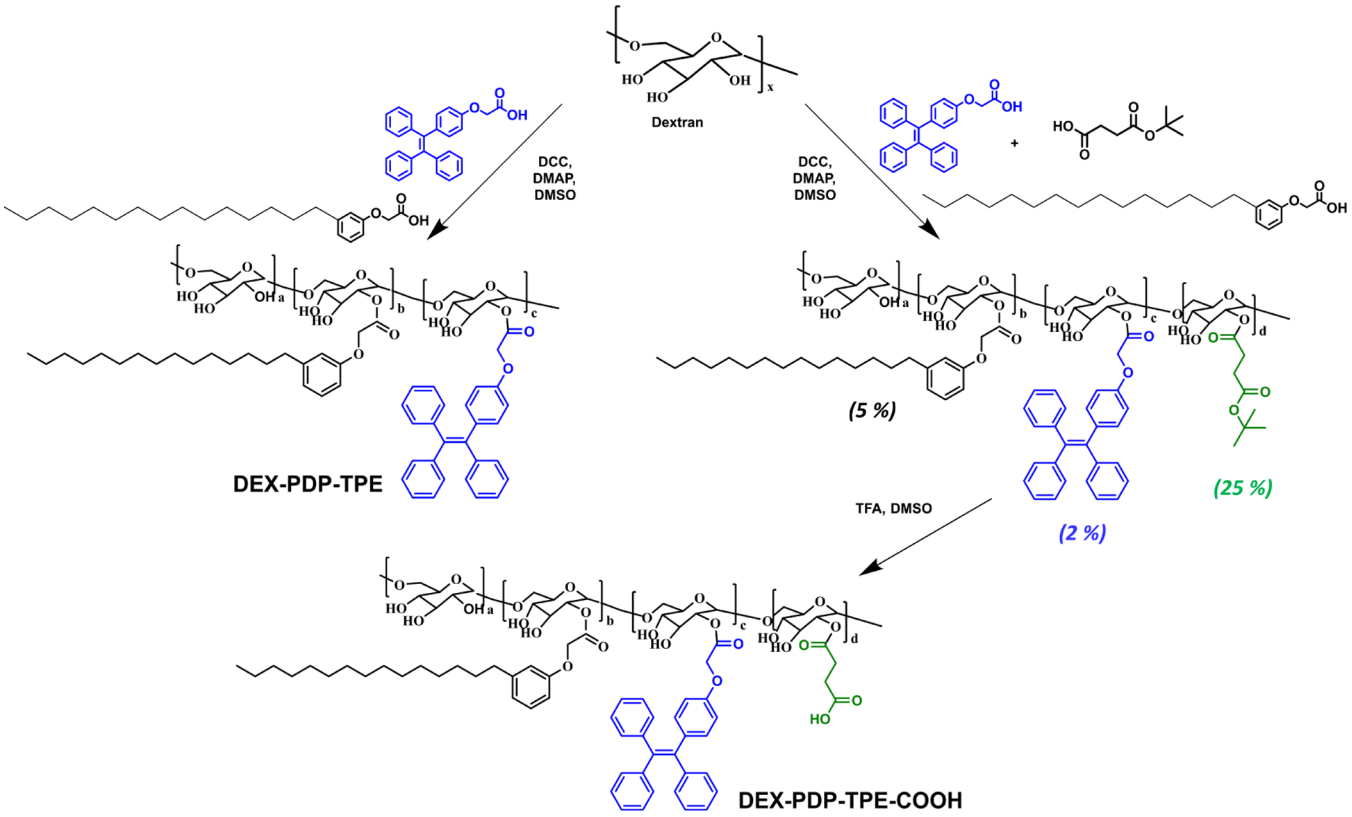


butyl ester group produced a carboxylic acid-substituted dextran derivate. The degree of substitution for PDP acid and TPE acid was calculated using $^1$H NMR, as shown in Figure S1, by comparing the proton intensity of aromatic protons with anomeric protons (4.6 ppm) of the dextran polysaccharide, giving a value of 5% for PDP and 2% for TPE. The degree of substitution for the SA group was calculated by comparing the proton intensity of the tertiary butyl group of the SA derivative with that of anomeric protons of the dextran polysaccharide, which came out as 25%. Alternatively, TPE acid and PDP acid were anchored simultaneously on the dextran to yield DEX−PDP−TPE (without carboxylic acid substitution) with a similar degree of substitution. The degree of substitution on the dextran is controlled by maintaining the equivalent ratio of PDP acid, TPE acid, and succinic ester in the feed. The degree of substitution increases linearly with the increasing equivalents of the respective acids in the feed. The dependence of the equivalent ratio in the feed versus amount incorporated has been studied in detail.[35] The mole equivalents of three acids SA, PDP, and TPE were maintained as 0.5, 0.25, and 0.06 in the feed with respect to each sugar unit in the dextran which led to the incorporation of 25, 5, and 2%, respectively, with respect to an average of 37 sugar repeating units in a dextran molecular weight of 6000 g/mol. The feed ratios of these acids are 8:4:1 for SA, PDP, and TPE which is different from the actual degree of substitution 12.5:2.5:1. This difference in substitution can be accounted for the difference in reactivity of the three acids (Scheme 1).

Self-assembly of a derivatized dextran polymer in aqueous medium resulted in polymersomes due to interdigitation of a long hydrophobic alkyl chain of PDP units.[37,38] The hydrophobic rigid TPE units acquired in the hydrophobic layer created by vesicular assemblies exhibited AIE with strong blue-luminescence due to RIM of aromatic rings, as shown in the schematic of Figure 2a. The vesicles are unique architectures with a well-separated hydrophobic bilayer and hydrophilic lumen or core. The hydrophobicity of the bilayer in the present case is high owing to the interdigitation of the PDP chains which leads to the formation of the bilayer. PDP molecules hence define the interior of the bilayer, making it more hydrophobic and thereby pushing water-loving groups outside facing the water environment. Furthermore, the inward folding of the bilayer to minimize surface tension leads to the formation of vesicles. Water is engulfed and forced inside the lumen during the process of inward folding, making the lumen or core more hydrophilic. In the present case, as the bilayer folds, it engulfs surrounding water molecules and this pushes the COOH−acid group on the periphery of the membrane to later only rest inside the hydrophilic lumen of the formed vesicle, as shown in Figure 2a. The minimum amount of PDP required to produce vesicular assembly is 5%, and the dextran derivative became water insoluble when the incorporation exceeds 10%, hampering its self-assembly process in water.[35] The polymer was dispersed in the solvent of varying DMSO and water to access AIE properties. The photoluminescence (PL) spectra of the polymer solution (OD = 0.1, $\lambda_{exc}$ = 340 nm) in the DMSO solvent showed emission maxima at 394 nm, corresponding to the monomeric emission peak. The intensity of the monomeric peak decreased as the water content increased from 0 to 100% with a simultaneous emergence of a new peak at 472 nm which can be attributed to the aggregated emission peak, as shown in Figure 2b. No variation was observed in absorbance maxima of the TPE chromophore for varying solvent composition (see Figure S2). The main reason for variation in PL intensity was AIE and not due to the difference in the molar absorptivity. The plot of


https://doi.org/10.1021/acspolymersau.1c00042
ACS Polym. Au 2022, 2, 181−193

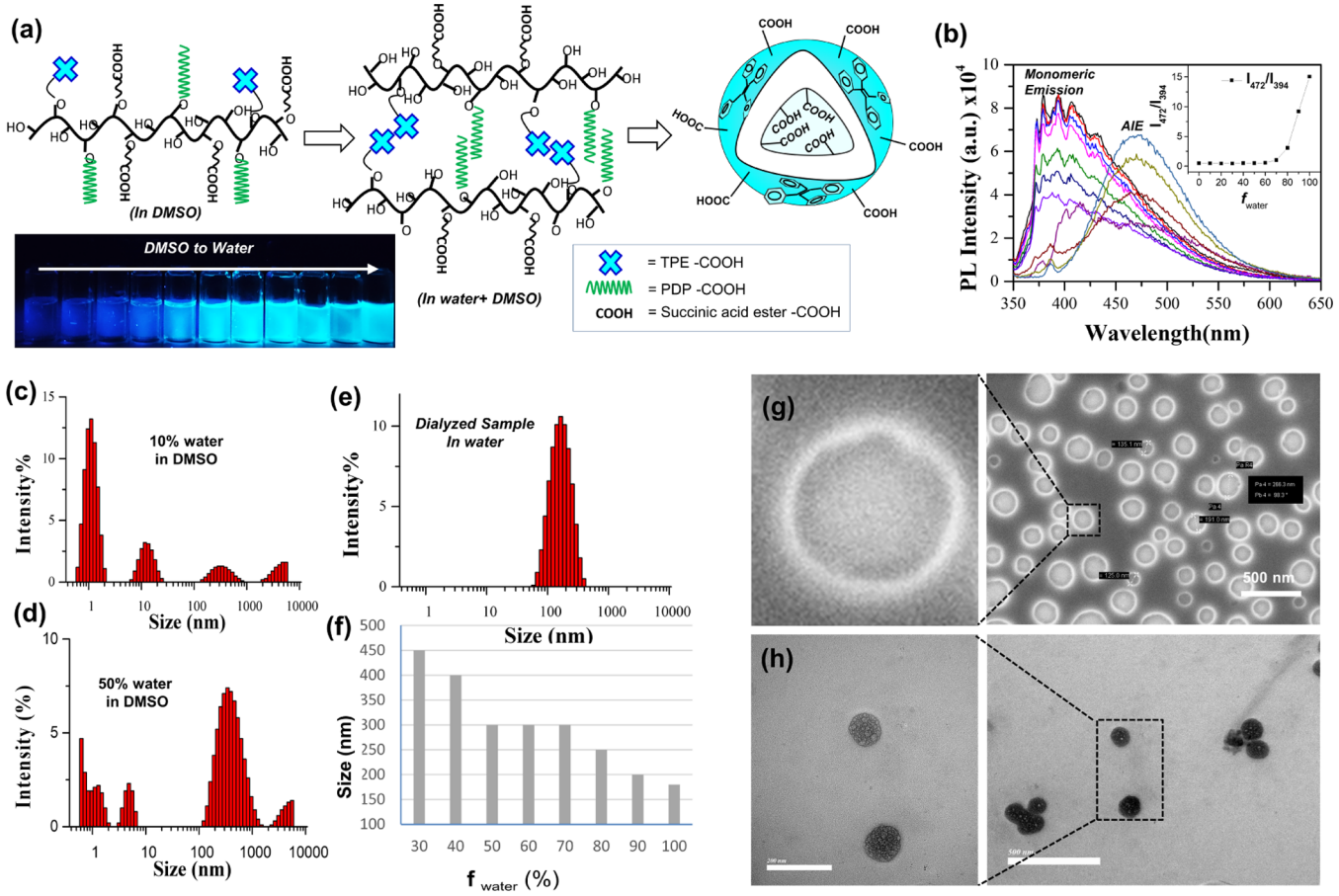


**Figure 2.** (a) Self-assembly of DEX−PDP−TPE−COOH. (b) Emission spectra of a polymer in the solvent DMSO + water mixture. The inset in the figure shows $I_{472}/I_{394}$ vs composition. DLS distribution for DEX−PDP−TPE−COOH in (c) 10% DMSO/water composition, (d) 50% DMSO/water composition, and (e) dialyzed water. (f) Bar plot showing variation of DLS size with varying water/DMSO composition. (g) FESEM and (h) HR-TEM data for DEX−PDP−TPE−COOH and the zoomed image.

ratio of intensity $I_{472}/I_{394}$ versus solvent composition clearly depicted a break point at 30% DMSO in water (inset, Figure 2b). Due to $\pi-\pi$ stacking of aromatic units, the intramolecular rotation of aromatic rings got restricted and resulted in new aggregated species which has emission at a higher wavelength compared to monomeric emission. Polysaccharide polymersome self-assembly is typically produced by the dialysis method by dissolving a polymer in the DMSO + water mixture and dialyzing against fresh water using a semipermeable membrane. In this process, DMSO was gradually removed from the dialysis tube which indirectly enhances the water content inside the dialysis membrane, forcing the polymer chains to undergo self-assembly. The interdigitization of hydrophobic unit (PDP chains in the present case) in water drives the system to form bilayer assembly. Subsequent folding of the bilayers and splitting of the large-size mother vesicles to smaller-size daughter vesicles helps minimize the surface tension and the process continues until tiny nanosize polymersomes are produced in the aqueous phase.[47,48] Therefore, the DMSO + water composition-dependent fluorescence data in Figure 2b are reflection of actual aggregation phenomena experienced by the DEX−PDP−TPE−COOH polymer during self-assembly inside the dialysis membrane. The exhibition of strong fluorescence in the presence of higher water content is a direct read out of the interchain aggregation of the DEX−PDP−TPE−COOH during the formation of blue-luminescent polymersome nanoassemblies.

To validate the DEX−PDP−TPE−COOH polymer self-assembly, dynamic light scattering (DLS) studies was performed for the polymer solution (0.1 mg/mL) in different solvent compositions (Figure S4). DLS plots showed that the polymer self-assembly was very poor in the DMSO-rich composition as evident from a multimodal distribution (10% water in DMSO, Figure 2c). In water-rich solvent compositions, the chains tend to aggregate in a higher order to produce compact nanoassemblies and the distribution began to center at 200 nm (see 50% water in DMSO samples, Figure 2d). The size distribution in the histogram became narrower with the further increase in the water environment (Figure S4) and the size matching with that of the completely dialyzed sample (in water, Figure 2e). The plot of DLS sizes in different solvent mixtures in Figure 2f clearly indicates the self-assembly of the polymer in a water-rich environment. The comparison of Figures 2b−d and S4 establishes that the enhancement in the AIE signal is driven by the formation of tiny polymersome nanoassemblies in water. Field emission scanning electron microscopy (FESEM) images of the dialyzed samples were recorded, and the images shown in Figure 2g showed a well-distinguished bilayer in good contrast to that of lumen. High-resolution transmission electron microscopy (HR-TEM) images in Figure 2h showed similar characteristics and lumen appeared to be porous. Polymer vesicles or polymersomes are


https://doi.org/10.1021/acspolymersau.1c00042
ACS Polym. Au 2022, 2, 181−193

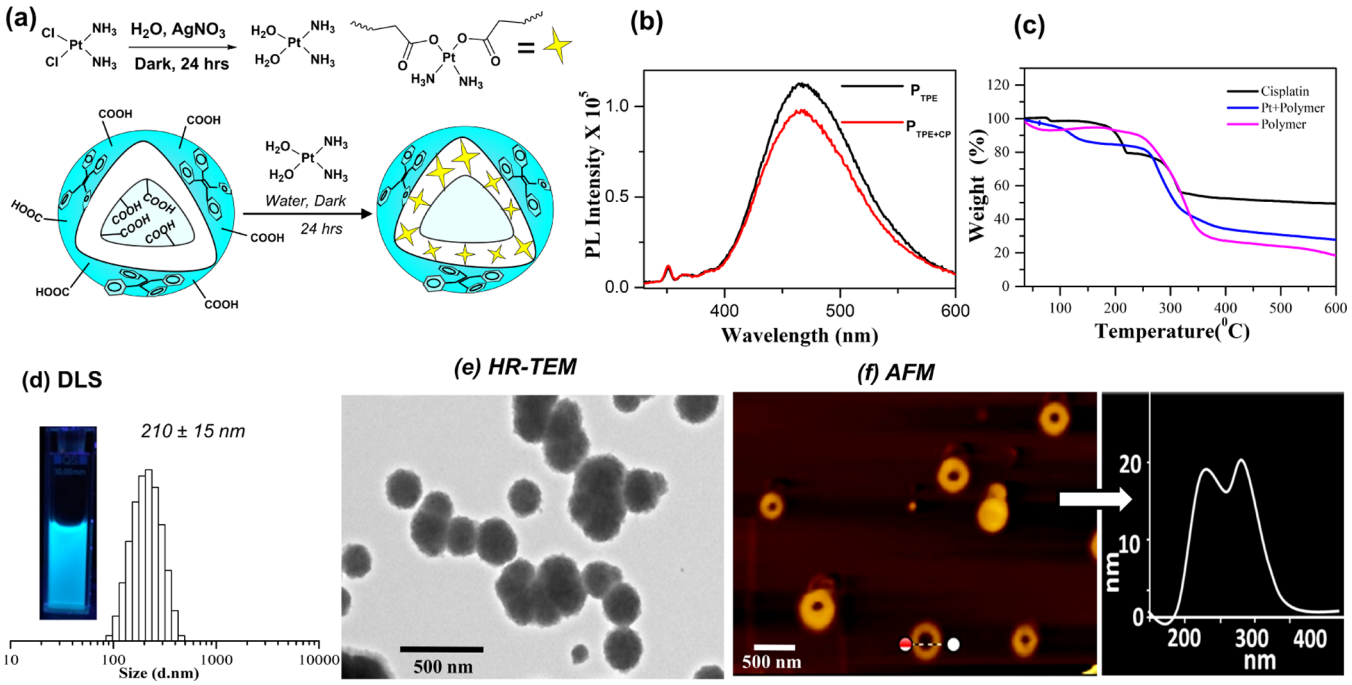


**Figure 3.** (a) Schematic showing cisplatin stitching of the dextran carboxylic acid derivative. (b) Fluorescence spectra of the DEX−PDP−TPE−COOH derivative before and after cisplatin conjugation. (c) TGA plot for dextran, Pt-stitched dextran, and free cisplatin. (d) DLS histograms, (e) HR-TEM image, and (f) AFM image of cisplatin-stitched DEX−PDP−TPE−COOH polymersomes.

mesmerizing architectures composed of a well-defined tightly packed hydrophobic bilayer membrane and a hydrophobic lumen. The versatility of polymersomes comes from their well-defined architecture emanating from appropriate balance between hydrophobic PDP tails and the hydrophilic glucose backbone of dextran. The interdigitation of long PDP tails leads to the formation of a bilayer, whose subsequent folding leads to the formation of structurally ordered vesicles of size less than 200 nm and a bilayer thickness of 2.45 nm, as confirmed via TEM analysis in earlier investigation.[35] The nature of chain packing in the bilayer was rationalized by resolving the single-crystal X-ray structure of its hydrophobic PDP unit.[47] The alkyl chains in PDP projected toward each other owing to like−like interactions, leading to the formation of a hydrophobic layer of thickness 29.2 Å or 2.92 nm. This matched well with the bilayer thickness of the vesicles obtained from the TEM analysis. Atomic force microscopy (AFM) showed the presence of a hollow cavity and a hard periphery which is characteristic of vesicular morphology. Such transitions were then captured via confocal fluorescence microscopy employing fluorescent rose bengal dye as a guest molecule loaded inside dextran vesicles. Initially, larger-sized disordered bilayer structures could be seen which became smaller as time elapsed. With larger-sized vesicles, the periphery could be clearly distinguished from the lumen but became indistinguishable as the size became smaller owing to resolution limits of the confocal instrument.[46] From all our previous studies, it was seen that the morphology remained vesicular even after drug encapsulation[35,38,40] or conjugation.[41,42] Our group had explored these nanovesicle architectures for multitude of drug delivery ranging from water-soluble chemotherapeutic drugs such as DOX,[35,38,40] cisplatin,[42] CPT,[35] and their cocktails for combination therapy[41,42] and extremely water-insoluble aurora kinase inhibitors MLN 8237 for inhibiting the anchorage-independent growth of cancer cells.[39] From these studies, it is clear that the vesicle or polymersome formation by the dextran-conjugated PDP is both thermodynamically and kinetically controlled for drug-delivery applications.

## Cisplatin-Stitched AIE Polymersomes

To conjugate the cisplatin drug on the polysaccharide backbone, a cisplatin aqua complex was made by treating cisplatin with silver nitrate in water for 24 h in the dark.[41] This aqua complex was then treated with an acid-functionalized polysaccharide derivative under basic conditions. The reaction for aqua complex formation and cisplatin stitching to the polymer backbone is schematically shown in Figure 3a. During cisplatin conjugation, one would anticipate a reduction in the log *P* value of the formed esters. Esters are known to have a more positive log *P* value, and hence, cisplatin has more preference for hydrophobic domains in the vesicles, as shown in Figure 3a. The photophysical properties of the fluorophore-tagged derivatives are imperative to study before their biological application. The derivatives in the present study are designed to show special AIE, and thus, it is important to study their photophysical properties to ensure their applicability for biomedical imaging. The emission properties before and after cisplatin stitching were monitored using a 340 nm excitation wavelength. The data in Figure 3b clearly indicate that both the polymersomes showed significant emission and confirm that the cisplatin stitching in these polymersomes does not hamper the AIE property of the fluorophore. The cisplatin stitching onto the polymer backbone was confirmed using three different techniques such as Fourier transform infrared (FT-IR), orthophenylene diamine (OPD) colorimetric assay, and thermogravimetric analysis (TGA). The FT-IR spectrum (see Figure S3) of acid-functionalized polysaccharide derivatives, where dextran has a carboxyl functional group and an ester functional group, showed a distinct peak at 1740 $cm^{-1}$ corresponding to the ester −C═O peak. Upon cisplatin


https://doi.org/10.1021/acspolymersau.1c00042
ACS Polym. Au 2022, 2, 181−193

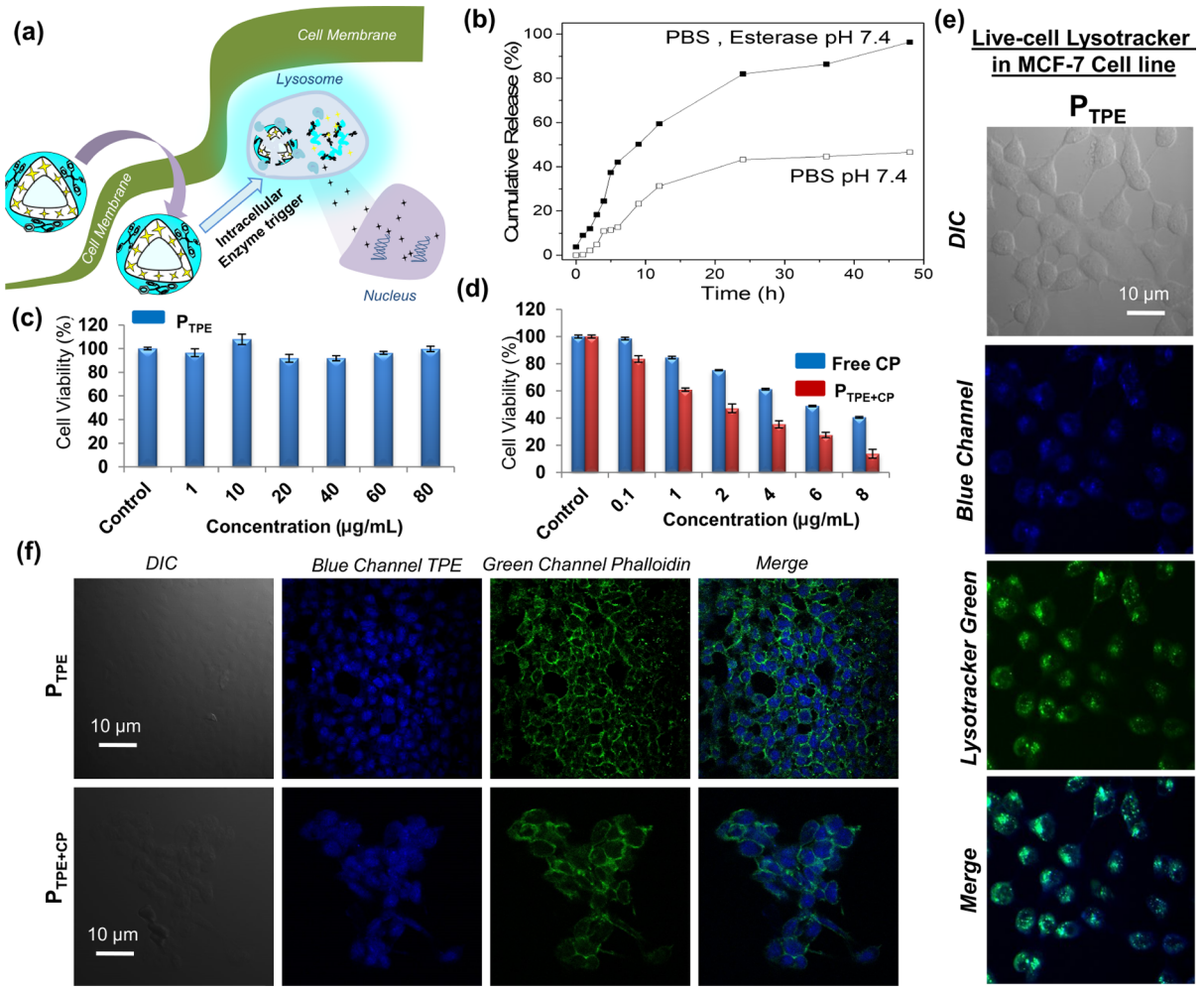


**Figure 4.** (a) Schematic showing enzyme-assisted release of the platinum drug from DEX−PDP−TPE−COOH. (b) Cisplatin release kinetics in the presence and absence of the esterase enzyme under phosphate-buffered saline conditions at pH = 7.4. (c) MTT experiment showing cell viability of $P_{TPE}$ polymersomes in MCF 7 cell lines. (d) Cell viability data for free cisplatin and $P_{TPE+CP}$ polymersomes in MCF 7 cell lines. (e) Live-cell Lysotracker experiment for $P_{TPE}$ polymersomes in MCF 7 cell lines. (f) Fixed-cell images showing the cellular uptake of $P_{TPE}$ and $P_{TPE+CP}$ polymersomes in MCF 7 cell lines, co-staining with phalloidin for visualization cellular actin and filaments.

complexation, these derivatives displayed a discrete stretching band at 1650 $cm^{-1}$ with respect to the Pt−O−C═O stretching frequency of the carboxylic acid functional group. Additionally, a distinct peak at around 480 $cm^{-1}$ corresponding to the Pt−O (metal alkoxide) bond stretching clearly appeared in the cisplatin-stitched derivatives.[54] To calculate the drug-loading content (DLC), OPD assay has been performed, wherein the cisplatin-stitched derivatives were treated with OPD solution in dimethylformamide and the reaction was allowed to happen at 80 °C for 2 h. Upon the OPD complexation with cisplatin, the formed OPD−cisplatin adduct showed a strong absorption peak at 706 nm. Using the Lambert−Beer's law, the amount of cisplatin stitched on the polymer backbone was calculated and the DLC was found to be 11.5%. Cisplatin drug exhibited two-step degradation in the TGA profile in Figure 3c, first at 220 °C and second at 330 °C corresponds to both ligands' degradation (overall 40% weight loss for ligands) below 400 °C and remained almost constant up to 800 °C for Pt metal content. The dextran polymer showed a sudden dip at 280 °C (∼80% weight loss). Typically, Pt−polymer conjugate degradation had started at 270 °C (degradation of ligand) and gradually decreased up to 70% weight loss up to 500 °C (degradation of polymer). Thereafter, up to 800 °C, it was constant showing the Pt metal content, as shown in Figure 3c. Based on TGA, platinum content in the Pt-stitched polymer was found to be ∼12%. The cisplatin-stitched polysaccharide derivative was dispersed in water, and the size of the nano-objects was measured using the DLS technique which showed a monomodal distribution of size around 210 ± 15 nm (Figure 3d). The photograph of the vial showed in Figure 3d represents a blue-colored transparent aqueous solution of cisplatin-stitched derivatives. The HR-TEM image in Figure 3e confirmed the existence of spherical nanoassemblies; however, it could not differentiate between the softer core and the harder periphery. This is owing to the high contrast offered by the presence of heavy metals such as cisplatin, thereby making it difficult to distinguish the core from the periphery. To confirm the polymersome nano-assembly in the cisplatin-stitched samples, the morphology of these nano-objects was studied using AFM. The principle of AFM relies on the dispersion of energy by the AFM tip when it taps the surface of the nano-object. The energy disputation becomes the direct readout for the softness or hardness of the surface. The center of the polymersomes is typically softer than the periphery which can clearly be seen from the elevated phase in the height profile diagram. Dip in this phase diagram


https://doi.org/10.1021/acspolymersau.1c00042
ACS Polym. Au 2022, 2, 181−193

corresponds to the soft region of the nano-object. A soft center and hard periphery point toward a vesicular morphology, as shown in Figure 3f (phase information shown by the height profile). The sizes of the polymersomes from AFM and HR-TEM were found to be 200 ± 20 and 210 ± 20 nm which matched well with sizes obtained from the DLS measurement data (Figure 3d). The polymersomes will hereafter be referred as "$P_{TPE+CP}$".

Since cisplatin stitching to the polymer backbone was performed via the ester bonds, it was important to study the effect of the enzyme activity on these polymersomes. Hence, enzyme-responsive release of cisplatin from these polymersomes was investigated in pH = 7.4 at 37 °C. The schematics showed in Figure 4a explains the enzymatic cleavage of the polymersomes and release of the cisplatin drug. The in vitro release kinetics was determined in the presence of 10 U of esterase enzyme and in phosphate-buffered solution (PBS) maintained at pH = 7.4 to monitor the release of cisplatin, as shown in Figure 4b. The amount of the cisplatin released was monitored by OPD colorimetric assay, and the details are given in the experimental section. From Figure 4b, it was observed that these cisplatin-stitched polymersomes showed a good stability in PBS 7.4 with about 30% after 12 h. Dialyzed samples are typically lyophilized and stored at 4 °C, and the stability of the cisplatin-stitched samples was found to be stable for more than 6 months. A release study is typically performed for 48 h and the 40% release was accounted for the partial complex destabilization of the Pt complex by the $Cl^-$ or phosphate ions present in the PBS.[55] When these polymersomes were treated with 10 U of the esterase enzyme, the enzyme triggered the release of the drug and almost 90% of the drug release was observed in 48 h. This experiment proved that the release of the cisplatin drug can be triggered using the esterase enzyme and the same effect is anticipated at the intracellular level. To evaluate the cytotoxic effect of the polysaccharide polymersomes ($P_{TPE}$), cisplatin-stitched polymersomes ($P_{TPE+CP}$), and free cisplatin on the human breast cancer MCF 7 cells, initially, the cells were treated with polysaccharide polymersomes and incubated for 72 h and the effect was studied using standard MTT assay. The results are shown in Figure 4c,d. It is evident from Figure 4c that $P_{TPE}$ was not toxic to the cells up to a concentration of 80 $\mu$g/mL, hence proving the noncytotoxic nature of the present design. Further cells were treated with free cisplatin and $P_{TPE+CP}$ and incubated for 72 h and the results are shown in Figure 4d. From the bar diagram in Figure 4d, it was observed that the free cisplatin drug was able to achieve only 60% cell killing and the 40% population was still alive even after 72 h of incubation. On the other hand, the cisplatin-stitched polysaccharide polymersomes could achieve more than 90% of cell killing, proving the fact that the polymersome platform is an excellent choice for cisplatin delivery to cancer cells. The enhanced cytotoxicity of the cisplatin conjugated to polymersomes can be attributed to the cleavage of polymersomes in the lysosomes of the cells.

To understand the uptake mechanism of these polymersomes, a Lysotracker experiment was performed. Cells were incubated with media containing $P_{TPE}$ for a time period of 60 min. The blue luminescence of $P_{TPE}$ emanating from the TPE unit attached to the polymersomes could be traced inside the cells when selectively excited using a 405 nm laser source and subsequent collection of emission intensity in the blue channel, as shown in Figure 4e. The cells were then co-stained with a Lysotracker dye DND 26 which specifically stains the lysosomes of the cells in comparison with another cytosolic organelle. The lysosomes are marked green due to the fluorescence coming from Lysotracker green. Interestingly, the green emission from the Lysotracker stain matches very well with the blue emission of the TPE chromophore (as shown by the merged image in yellow color) tagged to $P_{TPE}$. This clearly suggests that $P_{TPE}$ are taken up inside the cells via the endocytosis pathway. Cellular uptake of $P_{TPE}$ and $P_{TPE+CP}$ was investigated in a fixed MCF 7 cell line and the data are shown in Figure 4f. The blue channel for both $P_{TPE}$ and $P_{TPE+CP}$ showed blue luminescence coming from TPE when excited using a 405 nm laser. This suggests that both $P_{TPE}$ and $P_{TPE+CP}$ exhibit a similar luminescence behavior inside the cells and that cisplatin conjugation has not altered the photophysical properties of TPE as also proved from photophysical studies performed for $P_{TPE+CP}$ and $P_{TPE}$, as shown in Figure 3b. Phalloidin staining for both the polymersomes was carried out. A uniform and intact cellular actin could be seen in green. The merged image showed that polymersomes were not stuck to the actins or filaments and were localized efficiently inside the cytoplasm, as shown in Figure 4f. The enhanced efficacy of $P_{TPE+CP}$ can be then attributed to the cleavage of the polymersomes inside the lysosome of the cells and subsequent release of the free cisplatin, leading to enhanced cell death. The enhanced efficacy of the $P_{TPE+CP}$ in MCF 7 cell line motivated us toward testing these polymersomes for loading and activity of other cytotoxic drugs such as DOX.

## DOX-Encapsulated Polymersomes

The TPE-conjugated dextran scaffold DEX−PDP−TPE (see Scheme 1, without −COOH group) was self-assembled in water to produce blue-luminescent polymersomes. The emission spectra of the polymer solution (for OD = 0.1, $\lambda_{exc}$ = 340 nm) in the DMSO + water solvent composition showed strong blue fluorescence in water with emission maxima at 460 nm with respect to the AIE from TPE (see Figure S5b). No significant changes were observed in the absorbance spectra of varying DMSO/water composition, as shown in Figure S5a. The plot of PL intensity versus the solvent composition is shown in Figure S5c, showing a clear break point at 50% of DMSO + water composition. DOX which is a red-luminescent water-soluble drug could be loaded in the blue-luminescent polymersomes. Encapsulation of the water-soluble anticancer drug DOX hydrochloride (DOX·HCl) in the polymersomes was carried out by the dialysis method using a semipermeable membrane having a molecular weight cutoff of 1000 g/mol. The unencapsulated drug molecules were removed by replenishing fresh water in the reservoir and carrying out dialysis for 48 h. The DLC and drug-loading efficiency of $P_{TPE+DOX}$ were found to be 3.8 and 60%, respectively. The DOX-loaded TPE polymersome is hereafter referred as $P_{TPE+DOX}$. Attempts were also made for the encapsulation of DOX in the carboxylic-substituted $P_{TPE}$ (used for cisplatin stitching); however, DLC was obtained almost similar so that it was not considered for further studies. The size of $P_{TPE+DOX}$ was determined by DLS as 220 ± 20 nm (see Figure S5d). FE-SEM (see Figure S5e) showed donut-like morphology which corresponds to the vesicular-like nature of the soft assembly. HR-TEM images (see Figure S5f) further confirmed the existence of spherical polymersome nanoassemblies as evident from a hollow center and a harder periphery which can be clearly seen as the contrast difference in the image. The physical encapsulation of DOX in $P_{TPE}$ yielded $P_{TPE+DOX}$


https://doi.org/10.1021/acspolymersau.1c00042
ACS Polym. Au 2022, 2, 181−193

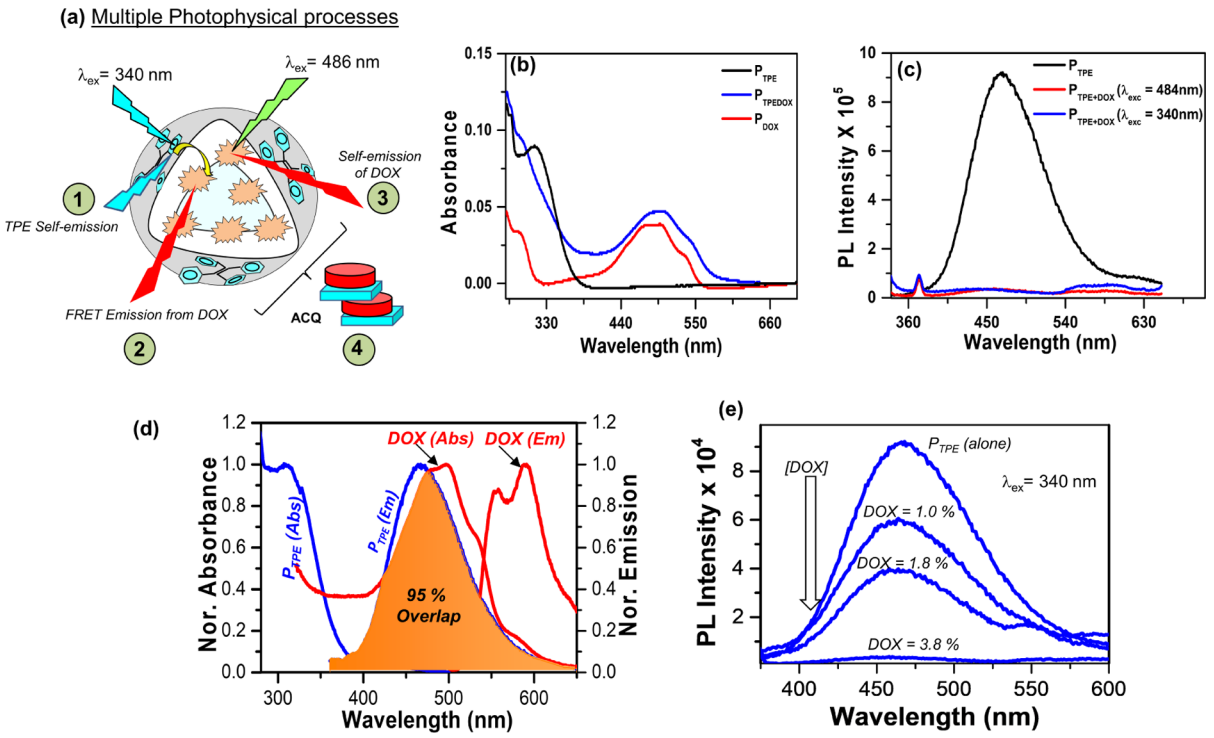


**Figure 5.** (a) Schematic representation of four different types of the photophysical process possible for the selective photoexcitation of TPE and DOX chromophores. (b) Absorbance spectra of $P_{TPE-DOX}$, $P_{TPE}$, and $P_{DOX}$ in an aqueous medium. The optical density (OD) of TPE and DOX·HCl was maintained as 0.1 and 0.05 in the samples. (c) Emission spectra of $P_{TPE+DOX}$, at TPE excitation (blue line), $P_{TPE+DOX}$, at DOX excitation (red line), and $P_{TPE}$, in aqueous medium. Emission spectra of $P_{TPE+DOX}$ and $P_{TPE}$ were recorded using $\lambda_{exc}$ = 340 nm, and $P_{DOX}$ was recorded using $\lambda_{exc}$ = 484 nm. (d) Plot showing overlap integral between emission of TPE and absorbance of DOX shaded in orange and (e) emission spectra of $P_{TPE+DOX}$ with different amounts of DOX loaded in their polymersome, spectra were recorded at $\lambda_{exc}$ = 340 nm.

polymersomes. It is quite interesting to understand the interaction of the blue-luminescent TPE molecule attached to the polymersome with that of physically encapsulated red-luminescent DOX as the guest molecule. We could anticipate the following physical process taking place between TPE and DOX which are (i) self-emission of TPE when excited at the TPE excitation wavelength (340 nm), (ii) fluorescent resonance energy transfer (FRET) emission between TPE and DOX in which TPE acts as a donor and DOX acts as an acceptor molecule, (iii) self-emission of DOX when excited at DOX (484 nm), and (iv) complete fluorescence quenching between TPE and DOX when excited at their respective excitation wavelength.

To understand the possible molecular interaction between DOX and TPE in $P_{TPE+DOX}$, the OD of TPE in $P_{TPE}$ and $P_{TPE+DOX}$ (see Figure 5b) was maintained as 0.1. The OD of TPE in control or empty polymersomes ($P_{TPE}$) was also maintained as 0.1. Upon photoexcitation of TPE at $\lambda_{exc}$ = 340 nm, the $P_{TPE}$ showed strong blue emission at 460 nm with respect to AIE in the aqueous medium (see Figure 5c). Interestingly, the photoexcitation of TPE at $\lambda_{exc}$ = 340 nm in $P_{TPE+DOX}$ exhibited complete fluorescence quenching of both TPE and DOX. The system was rendered completely dark. Furthermore, the selective photoexcitation of DOX (at $\lambda_{exc}$ = 484 nm) in $P_{TPE+DOX}$ also did not show red emission from DOX, as shown in Figure 5c. This observation confirmed that both DOX and TPE chromophores underwent strong ACQ, resulting in the complete turn-off of emissions from both DOX and TPE in the polymersome nanoassemblies. TPE and DOX were reported to be very good FRET pairs in earlier reports,[49−53] and they were known to exhibit complete fluorescent turn-off in the aggregated state. Therefore, the complete turn-off of the fluorescent signal in the $P_{TPE+DOX}$ was attributed to FRET between TPE and DOX. TPE could transfer its energy to DOX as seen from the reduction in the emission intensity of TPE. However, the transferred energy did not cause an enhancement in the emission from DOX. This can be attributed to the strong $\pi-\pi$ interaction between the DOX molecules, causing complete fluorescence quenching.[49−53] Strong bimolecular quenching like the one observed here depends on the overlap between the donor and the quencher/acceptor of energy levels. The emission spectra of TPE overlap very well with the absorbance spectra of DOX. A 95% overlap integral is shown in orange in Figure 5d. To prove ACQ hypothesis for complete fluorescence quenching, control experiments were carried out and these details are shown in Figure 5e. Any ACQ process is highly driven by the composition of the quencher species (DOX in the present case); thus, the amount of DOX is varied with various degrees of loading (DLC values) to study the ACQ between TPE and DOX (it is important to note that the amount of TPE is fixed in the polymersome). The emission spectra of TPE were recorded for $P_{TPE+DOX}$ samples having different amounts of DOX loading content as 1.0, 1.8, and 3.8% and the data are shown in Figure 5e. As expected, the AIE from the TPE chromophores in the polymersome decreased with the increase in the amount of DOX loading. This experiment suggests that high DOX loading in the polymersome is essential for strong molecular interaction between DOX and TPE.

Enzyme trigger is employed to disassemble the polymersome via the cleavage of the aliphatic ester linkages that connect the hydrophobic PDP to the hydrophilic dextran


https://doi.org/10.1021/acspolymersau.1c00042
ACS Polym. Au 2022, 2, 181−193

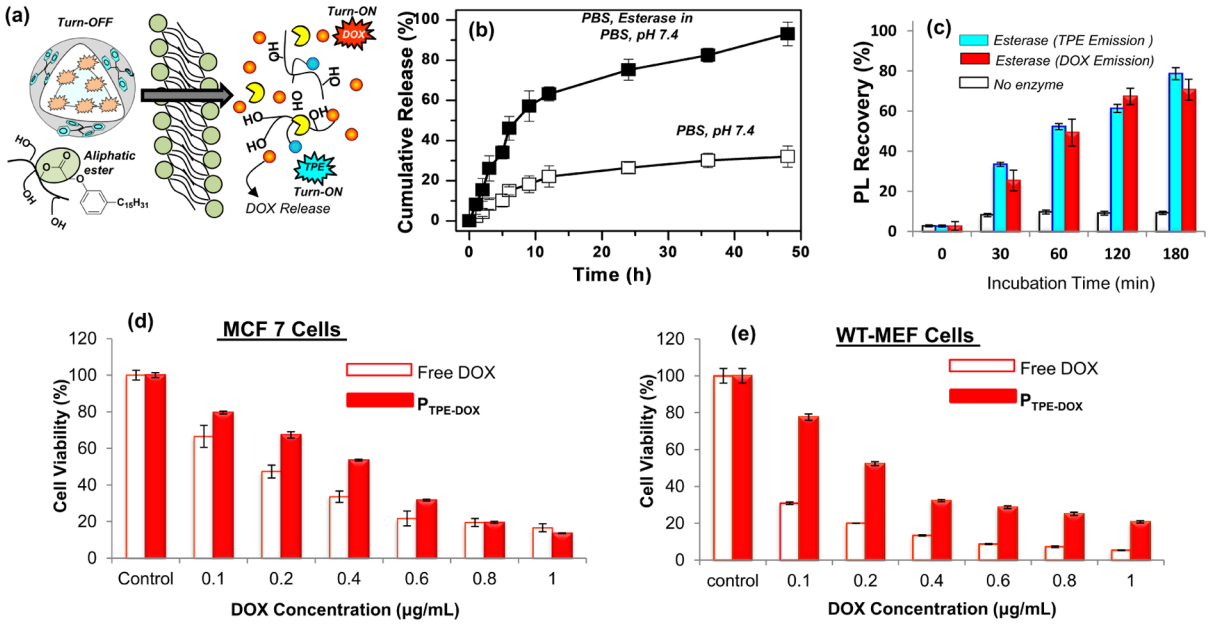


**Figure 6.** (a) Schematic showing the enzyme-assisted cleavage of polymersomes at the intracellular level leading to a fluorescence turn-off to turn-on system. (b) Cumulative drug-release profile of $P_{TPE+DOX}$ dispersed in PBS 7.4 both in the presence and absence of the esterase enzyme. (c) Bar diagram showing the fluorescence retrieval in a time-dependent manner in $P_{TPE+DOX}$ in the presence and absence of the enzyme. MTT data for $P_{TPE+DOX}$ and free DOX in (d) MCF 7 and (e) WT MEF cell lines.

backbone; as a result, the enzyme trigger can be employed as a switch to modulate the fluorescence activity of $P_{TPE+DOX}$ at the intracellular level, as shown in Figure 6a. $P_{TPE+DOX}$ was subjected to enzymatic disassembly using the horse liver esterase enzyme under in vitro conditions by the dialysis method.[35] A control experiment was also carried out in the absence of the esterase enzyme. The cumulative drug release was plotted against the incubation time and is shown in Figure 6b. It was also observed that $P_{TPE+DOX}$ polymersomes in PBS at pH 7.4 exhibited slight leaching (<20%) due to the influence of ions present in PBS. In the presence of the enzyme, the polymersomes underwent enzymatic disassembly and released 95% of DOX. Enzyme trigger was employed to study the extent of the fluorescence recoveries of both TPE and DOX from its ACQ-induced turn-off in $P_{TPE+DOX}$ polymersomes. In the presence of the enzyme, the TPE emission (see Figure S6a) and the DOX emission (see Figure S6b) were recovered completely within 3 h. This confirmed the turn-off → turn-on process in the $P_{TPE+DOX}$ polymersomes. In the absence of the esterase enzyme (in PBS at pH 7.4, see Figure S6c), neither the TPE emission nor the DOX emission recovery was noticed. The bar diagram in Figure 6c quantifies the enzyme-responsive fluorescence recovery from $P_{TPE+DOX}$, and it was found that the emission intensities of TPE and DOX were recovered almost 80% in a time-dependent manner compared to that of no enzyme control which stayed constant. This property makes it significant for turn-off → turn-on bioimaging probes. The fluorescence recovery experiments using $P_{TPE+DOX}$ polymersomes were also studied for other enzymes such as papain, trypsin, $\alpha$-chymotrypsin, and intracellular species such as glutathione (see Figure S7). Among all these enzymes, the esterase enzyme seems to be exhibiting the maximum efficiency for the cleavage of the aliphatic ester chemical linkages that connect the PDP at the dextran backbone. MTT assay was employed to study the cytotoxicity of the polymersomes ($P_{TPE}$) in human breast cancer cells (MCF 7) and the data are shown Figure 6d. MTT data in wild-type mouse embryonic fibroblast (WT-MEF) cell lines are given in Figure 6e. The free drug exhibited 80% cell death at a concentration of 1 $\mu$g/mL with an IC 50 value of 0.2 $\mu$g/mL. $P_{TPE+DOX}$ too exhibited 80% cell killing at 1 $\mu$g/mL with an IC 50 value of 0.40 $\mu$g/mL. Hence, the killing offered by $P_{TPE+DOX}$ is comparable to that of the free drug. The efficacy of the free drug and drug-loaded polymer is equivalent, which is an aided advantage as polymeric encapsulation did not alter/reduce the drug efficacy. $P_{TPE+DOX}$ exhibited comparatively less killing in WT-MEF cells as compared to free DOX. The polymersomes displayed similar efficacy as compared to the free drug and could also be effectively tracked inside the cells, giving important insights into enzyme-assisted drug delivery of the DOX drug.

## Live-Cell Bioimaging

Time-dependent cellular uptake experiments were carried out using the live-cell imaging technique to study the fluorescent "turn-off → turn-on" of the polymersome $P_{TPE+DOX}$. Breast cancer cells were treated with polymersomes by varying the incubation from 1 to 240 min using a four-well live-cell chamber and was imaged using a confocal instrument equipped with a stage incubator which was maintained at 37 °C and 5% $CO_2$ throughout the experiment. The TPE chromophore was excited with a 405 nm laser, and the images were captured in the range of the 415−510 nm window. DOX was excited with a 488 nm laser, and the images were captured in 510−720 nm. The live-cell imaging setup, equipped with an incubator, allowed us to capture images continuously from 1 to 45 min using a single well of a four-well live-cell chamber; however, for a longer incubation time (1 h and above), $P_{TPE+DOX}$ was administered to the cells in the remaining three wells of live-cell chambers and preincubated prior to imaging. Live-cell images recorded at various time intervals are shown in Figure 7a. The images captured for the TPE and DOX excitation are shown in the second and third rows, respectively. The merged


https://doi.org/10.1021/acspolymersau.1c00042
ACS Polym. Au 2022, 2, 181−193

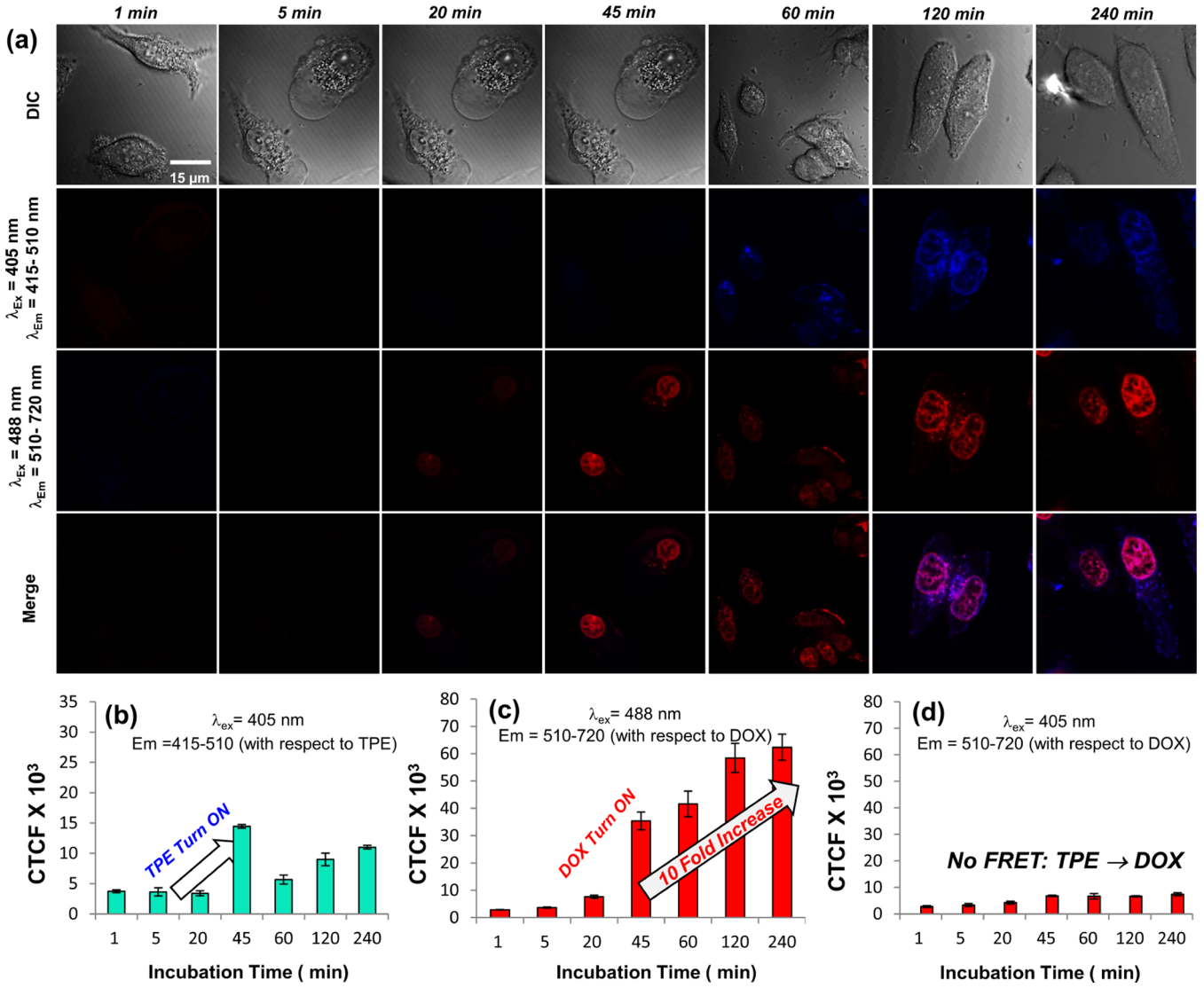


**Figure 7.** (a) Live-cell imaging for $P_{TPE+DOX}$. Excitation wavelength = 405 nm laser, collection of TPE emission in the blue channel (415−510 nm); collection of DOX emission in the red channel (510−720 nm); merged panel for the red and blue channel, as shown as magenta color. (b) CTCF calculation for the TPE channel showing fluorescence turn-on in a time-dependent manner. (c) CTCF plot for the DOX channel. (d) CTCF plot for no FRET channel, excitation source 405 nm laser, and collection in the FRET channel (510−720 nm).

image in the last row depicts the co-localization of both TPE and DOX chromophores together at the intracellular level. The images clearly showed that both TPE and DOX were completely in the turn-off state initially and then slowly turned-on with an increase in the incubation time. $P_{TPE+DOX}$ polymersomes initially are present in the turn-off stage at the intracellular level in the cytosol. Cellular uptake of the polymersome occurs very quickly (<5 min); thus, the longer duration taken up by the $P_{TPE+DOX}$ polymersomes to turn-on (45−60 min) in the present investigation is primarily attributed to the ACQ. Over a period of time, the lysosomal enzymatic disassembly of polymersomes triggered the isolation of the TPE and DOX chromophores. This, in turn, showed the turn-on of DOX and TPE self-emission in the cellular level. Since DOX is the DNA-intercalating drug, the close observation of the red emission in the cells clearly showed the increase in the DOX concentration at the nucleus with the increase in the incubation time. $P_{TPE+DOX}$ was excited using 405 nm (TPE excitation); however, the images were captured at DOX emission (from 510 to 720 nm, see Figure S8) to trace the FRET phenomena, if any occurred in the $P_{TPE+DOX}$ polymersomes at the intracellular level. Interestingly, the selective photoexcitation did not show any significant emission from DOX (see Figure S8) as noticed in the photophysical experiments shown in Figure 5c. Hence, it can be categorically ruled out that FRET phenomena did not occur between TPE and DOX containing the $P_{TPE+DOX}$ polymersomes at the intracellular level due to the isolation of donor and acceptor species. Corrected total cell fluorescence (CTCF) values were estimated and plotted, as shown in Figure 7b−d. In Figure 7b, TPE exhibited the turn-on blue emission almost 2−3-fold at the intracellular level with the increase in incubation time. DOX (in Figure 7c) exhibited turn-on red fluorescence almost by 8−10-fold.

This enhancement is significant enough to monitor the real-time drug release at the intracellular level. In Figure 7d, the CTCF data, calculated from the control experiment in Figure S8, showed that there is no FRET between DOX and TPE in the polymersomes at the intracellular level. This implies that the custom-designed $P_{TPE+DOX}$ polymersome is an excellent


https://doi.org/10.1021/acspolymersau.1c00042
ACS Polym. Au 2022, 2, 181−193

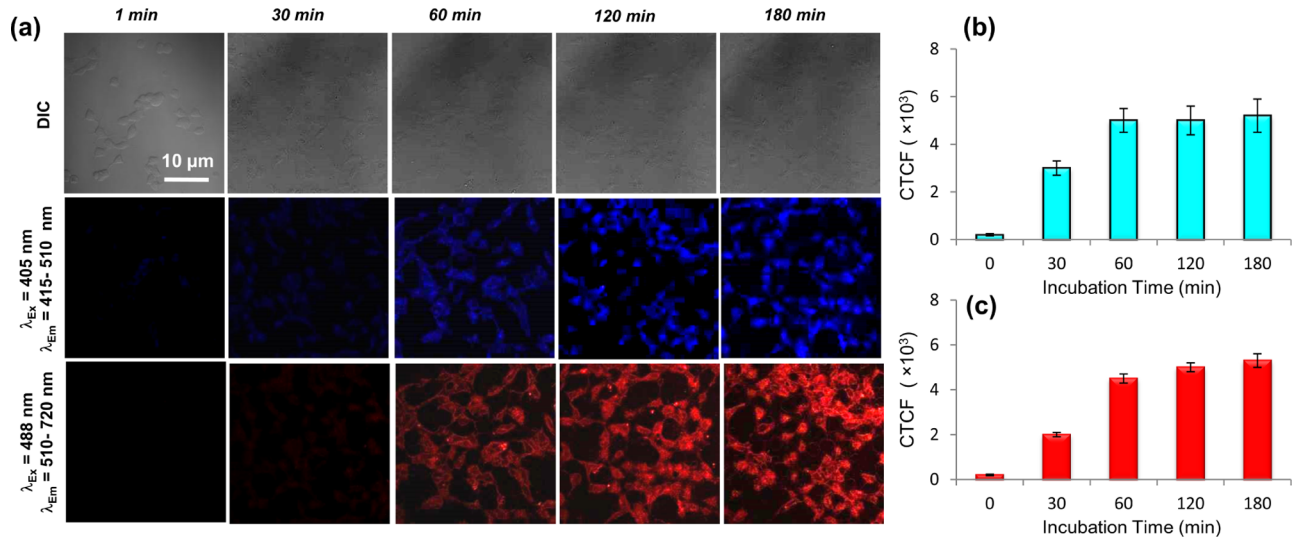


**Figure 8.** (a) Time-dependent fixed-cell confocal microscope images of $P_{TPE+DOX}$ polymersomes in the MCF 7 breast cancer cell line. (b) Bar plot showing CTCF for the emission recovery of TPE with time when excited using a 405 nm laser. (c) Bar plot showing CTCF for the emission recovery of DOX with time when excited using a 488 nm laser.

candidate to exhibit complete turn-off of DOX emission at the extracellular level (or under storage) and behave as a turn-on fluorescence switch to monitor polymersome disassembly in lysosomes and subsequent accumulation of DOX at the nucleus in a time-dependent manner. The proof of concept of capability of the polymersome design was also validated in fixed-cell confocal imaging in the breast cancer cell line (MCF 7). The fluorescence turn-on process in $P_{TPE+DOX}$ was studied in MCF-7 cells and data are shown in Figure 8a. The first panel represents the TPE blue channel (415−510 nm) followed by the TPE excitation at a 405 nm laser, and the second panel represents the red channel (510−720 nm) with respect to DOX emission when excited at a 488 nm laser. It is very clear from the images that the polymersome $P_{TPE+DOX}$ was in the "turn-off" state up to 60 min with no appreciable emission emanating either from TPE or DOX. This observation is attributed to the ACQ process between TPE and DOX, as explained earlier in Figure 5c. With the increase in the incubation time, there was a gradual increase in the emission intensity of both TPE and DOX, signifying the disassembly process at the intracellular level. CTCF of fluorescence recovery for TPE and DOX chromophores is plotted in Figure 8b,c, respectively. The complete emission recovery was observed only after 2 h of incubation. The current design holds promise for an enzyme-responsive theranostic probe in fixed-cell imaging.

## CONCLUSIONS

A class of dextran-based trackable universal polymersomes was synthesized and was successfully demonstrated as efficient drug-delivery vectors for the delivery of two different classes of drugs. The polymersomes were trackable owing to their blue-luminescent properties. The chemical modification of these polymersomes yielded carboxylic acid-functionalized scaffolds which can be used for conjugating the cisplatin drug. The cisplatin-conjugated, blue-luminescent polymersomes entered cells via endocytosis as confirmed by the Lysotracker experiment and were able to achieve 95% cell death in MCF 7 cancer cell lines. The efficacy of the cisplatin-conjugated polymersomes enhanced in comparison with the free drug. The blue luminescence emanating from the cisplatin-conjugated polymersomes made them traceable inside the cells which is otherwise not possible with the drug alone. The versatility of polymersomes could be enhanced by loading $P_{TPE}$ polymersomes with a well-known cytotoxic drug DOX. The physical interaction of the blue chromophore TPE with the red luminescent drug DOX leads to fluorescence quenching which was confirmed via various photophysical techniques. This turn-off probe can be selectively turned-on in response to cellular enzymes such as esterase as depicted in vitro. The enzyme-mediated rapture of polymersomes turned back the fluorescence of TPE and DOX as they moved apart. The accumulation of DOX in the nucleus of the cells and TPE-tagged polymersomes continued to be localized inside the cytoplasm which sheds light on the delivery mechanism of this scaffold. A commendable efficacy was achieved in MCF 7 cancer cell lines. The polymersome scaffold not only retained the efficacy of two different classes of drug molecules but also could be traced inside the cell, a feature not accomplished before. This class of universal polymersomes capable of loading different classes of drugs has a bright opportunity in future theragnostic research.

## ASSOCIATED CONTENT

### Supporting Information

The Supporting Information is available free of charge at https://pubs.acs.org/doi/10.1021/acspolymersau.1c00042.

$^1$H NMR of the synthesized compounds, absorbance data, enzyme response data, FTIR data for cisplatin conjugation, an FESEM and AFM data for $P_{TPE+DOX}$ (PDF)

## AUTHOR INFORMATION

### Corresponding Author

**Manickam Jayakannan** − *Department of Chemistry, Indian Institute of Science Education and Research (IISER Pune)*[RINGGOLD], *Pune 411008 Maharashtra, India;* orcid.org/0000-0001-7699-2016; Email: jayakannan@iiserpune.ac.in



https://doi.org/10.1021/acspolymersau.1c00042
*ACS Polym. Au* 2022, 2, 181−193

## Authors

**Mishika Virmani** − *Department of Chemistry, Indian Institute of Science Education and Research (IISER Pune)[RINGGOLD], Pune 411008 Maharashtra, India*

**Nilesh Umakant Deshpande** − *Department of Chemistry, Indian Institute of Science Education and Research (IISER Pune)[RINGGOLD], Pune 411008 Maharashtra, India*

**Shahidkhan Pathan** − *Department of Chemistry, Indian Institute of Science Education and Research (IISER Pune)[RINGGOLD], Pune 411008 Maharashtra, India*

Complete contact information is available at: https://pubs.acs.org/10.1021/acspolymersau.1c00042


## Author Contributions

M.V. and N.U.D. contributed equally to this paper. The manuscript was written through contributions of all authors. All authors have given approval to the final version of the manuscript. The authors declare no competing financial interest.


## Funding

The authors thank research grant from Science and Engineering Research Board (SERB), project no. CRG/2019/000496, New Delhi, India.


## Notes

The authors declare no competing financial interest.


## ■ ACKNOWLEDGMENTS

S.P. thanks UGC, New Delhi, India, for Senior Research Fellowship. We thank IISER Pune microscopy facility for cellular imaging.


## ■ REFERENCES


(1) Iqbal, S.; Blenner, M.; Alexander-Bryant, A.; Larsen, J. Polymersomes for Therapeutic Delivery of Protein and Nucleic Acid Macromolecules: From Design to Therapeutic Applications. *Biomacromolecules* **2020**, *21*, 1327−1350.

(2) Yin, Q.; Shen, J.; Zhang, Z.; Yu, H.; Chen, L.; Gu, W.; Li, Y. Multifunctional Nanoparticles Improve Therapeutic Effect for Breast Cancer by Simultaneously Antagonizing Multiple Mechanisms of Multidrug Resistance. *Biomacromolecules* **2013**, *14*, 2242−2252.

(3) Bobrin, V. A.; Lin, Y.; He, J.; Qi, Y.; Gu, W.; Monteiro, M. J. Therapeutic Delivery of Polymeric Tadpole Nanostructures with High Selectivity to Triple Negative Breast Cancer Cells. *Biomacromolecules* **2020**, *21*, 4457−4468.

(4) Pattni, B. S.; Chupin, V. V.; Torchilin, V. P. New Developments in Liposomal Drug Delivery. *Chem. Rev.* **2015**, *115*, 10938−10966.

(5) Jin, Q.; Deng, Y.; Chen, X.; Ji, J. Rational Design of Cancer Nanomedicine for Simultaneous Stealth Surface and Enhanced Cellular Uptake. *ACS Nano* **2019**, *13*, 954−977.

(6) Arcos, D.; López-Noriega, A.; Ruiz-Hernández, E.; Terasaki, O.; Vallet-Regí, M. Ordered Mesoporous Microspheres for Bone Grafting and Drug Delivery. *Chem. Mater.* **2009**, *21*, 1000−1009.

(7) Gupta, U.; Agashe, H. B.; Asthana, A.; Jain, N. K. Dendrimers: Novel Polymeric Nanoarchitectures for Solubility Enhancement. *Biomacromolecules* **2006**, *7*, 649−658.

(8) Rial-Hermida, M. I.; Rey-Rico, A.; Blanco-Fernandez, B.; Carballo-Pedrares, N.; Byrne, E. M.; Mano, J. F. Recent Progress on Polysaccharide-Based Hydrogels for Controlled Delivery of Therapeutic Biomolecules. *ACS Biomater. Sci. Eng.* **2021**, *7*, 4102−4127.

(9) Katterman, C.; Pierce, C.; Larsen, J. Combining Nanoparticle Shape Modulation and Polymersome Technology in Drug Delivery. *ACS Appl. Bio Mater.* **2021**, *4*, 2853−2862.

(10) Lale, S. V.; Aswathy, R. G.; Aravind, A.; Kumar, D. S.; Koul, V. AS1411 Aptamer and Folic Acid Functionalized pH-Responsive ATRP Fabricated pPEGMA-PCL-pPEGMA Polymeric Nanoparticles for Targeted Drug Delivery in Cancer Therapy. *Biomacromolecules* **2014**, *15*, 1737−1752.

(11) Moulahoum, H.; Ghorbanizamani, F.; Zihnioglu, F.; Timur, S. Surface Biomodification of Liposomes and Polymersomes for Efficient Targeted Drug Delivery. *Bioconjugate Chem.* **2021**, *32*, 1491−1502.

(12) Meng, F.; Zhong, Z.; Feijen, J. Stimuli-Responsive Polymersomes for Programmed Drug Delivery. *Biomacromolecules* **2009**, *10*, 197−209.

(13) Vargason, A. M.; Anselmo, A. C.; Mitragotri, S. The evolution of commercial drug delivery technologies. *Nat. Biomed. Eng.* **2021**, *5*, 951−967.

(14) Mitchell, M. J.; Billingsley, M. M.; Haley, R. M.; Wechsler, M. E.; Peppas, N. A.; Langer, R. Engineering precision nanoparticles for drug delivery. *Nat. Rev. Drug Discovery* **2021**, *20*, 101.

(15) Browning, R. J.; Reardon, P. J. T.; Parhizkar, M.; Pedley, R. B.; Edirisinghe, M.; Knowles, J. C.; Stride, E. Drug Delivery Strategies for Platinum-Based Chemotherapy. *ACS Nano* **2017**, *11*, 8560−8578.

(16) Frenkel, V.; Etherington, A.; Greene, M.; Quijano, J.; Xie, J.; Hunter, F.; Dromi, S.; Li, K. C. P. Delivery of Liposomal Doxorubicin (Doxil) in a Breast Cancer Tumor Model: Investigation of Potential Enhancement by Pulsed-High Intensity Focused Ultrasound Exposure. *Acad. Radiol.* **2006**, *13*, 469−479.

(17) Kim, E. S.; Lu, C.; Khuri, F. R.; Tonda, M.; Glisson, B. S.; Liu, D.; Jung, M.; Hong, W. K.; Herbst, R. S. A phase II study of STEALTH cisplatin (SPI-77) in patients with advanced non-small cell lung cancer. *Lung Cancer* **2001**, *34*, 427−432.

(18) Veal, G. J.; Griffin, M. J.; Price, E.; Parry, A.; Dick, G. S.; Little, M. A.; Yule, S. M.; Morland, B.; Estlin, E. J.; Hale, J. P.; Pearson, A. D. J.; Welbank, H.; Boddy, A. V. A phase I study in paediatric patients to evaluate the safety and pharmacokinetics of SPI-77, a liposome encapsulated formulation of cisplatin. *Br. J. Cancer* **2001**, *84*, 1029−1035.

(19) Mammen, M.; Choi, S.-K.; Whitesides, G. M. Polyvalent Interactions in Biological Systems: Implications for Design and Use of Multivalent Ligands and Inhibitors. *Angew. Chem., Int. Ed.* **1998**, *37*, 2754−2794.

(20) Davis, A. P. Sticking to Sugars. *Nature* **2010**, *464*, 169−170.

(21) Salatin, S.; Khosroushahi, A. Y. Overviews on the cellular uptake mechanism of polysaccharide colloidal nanoparticles. *J. Cell. Mol. Med.* **2017**, *21*, 1668−1686.

(22) Bhattacharya, K.; Banerjee, S. L.; Das, S.; Samanta, S.; Mandal, M.; Singha, N. K. REDOX Responsive Fluorescence Active Glycoploymer Based Nanogel: A Potential Material for Targeted Anticancer Drug Delivery. *ACS Appl. Bio Mater.* **2019**, *2*, 2587−2599.

(23) Feiner-Gracia, N.; Mares, A. G.; Buzhor, M.; Rodriguez-Trujillo, R.; Marti, J. S.; Amir, R. J.; Pujals, S.; Albertazzi, L. Real-Time Ratiometric Imaging of Micelles Assembly State in a Microfluidic Cancer-on-a-Chip. *ACS Appl. Bio Mater.* **2021**, *4*, 669−681.

(24) Parthiban, C.; Masilamani, P.; Reddy, L. V. K.; Sen, D.; Singh, N. D. P. Single-Component Fluorescent Organic Nanoparticles with Four-Armed Phototriggers for Chemo-Photodynamic Therapy and Cellular Imaging. *ACS Appl. Nano Mater.* **2019**, *2*, 3728−3734.

(25) Yu, T.; Zhuang, W.; Su, X.; Ma, B.; Hu, J.; He, H.; Li, G.; Wang, Y. Dual-Responsive Micelles with Aggregation-Induced Emission Feature and Two-Photon Aborsption for Accurate Drug Delivery and Bioimaging. *Bioconjugate Chem.* **2019**, *30*, 2075−2087.

(26) Dong, Z.; Bi, Y.; Cui, H.; Wang, Y.; Wang, C.; Li, Y.; Jin, H.; Wang, C. AIE Supramolecular Assembly with FRET Effect for Visualizing Drug Delivery. *ACS Appl. Mater. Interfaces* **2019**, *11*, 23840−23847.

(27) Jiang, Y.; Hadjichristidis, N. Tetraphenylethene-Functionalized Polyethylene-Based Polymers with Aggregation-Induced Emission. *Macromolecules* **2019**, *52*, 1955−1964.

(28) Birks, J. B., Ed. *Photophysics of Aromatic Molecules*; Wiley: London, 1970.

(29) Leung, N. L. C.; Xie, N.; Yuan, W.; Liu, Y.; Wu, Q.; Peng, Q.; Miao, Q.; Lam, J. W. Y.; Tang, B. Z. Restriction of Intramolecular Motions: The General Mechanism behind Aggregation-Induced Emission. *Chem.—Eur. J.* **2014**, *20*, 15349−15353.
(30) Jin, Y.; Song, L.; Su, Y.; Zhu, L.; Pang, Y.; Qiu, F.; Tong, G.; Yan, D.; Zhu, B.; Zhu, X. Oxime Linkage: A Robust Tool for the Design of pH-Sensitive Polymeric Drug Carriers. *Biomacromolecules* **2011**, *12*, 3460−3468.
(31) Han, S.; Lee, J.; Jung, E.; Park, S.; Sagawa, A.; Shibasaki, Y.; Lee, D.; Kim, B.-S. Mechanochemical Drug Conjugation via pH-Responsive Imine Linkage for Polyether Prodrug Micelles. *ACS Appl. Bio Mater.* **2021**, *4*, 2465−2474.
(32) Gu, Y.; Zhong, Y.; Meng, F.; Cheng, R.; Deng, C.; Zhong, Z. Acetal-Linked Paclitaxel Prodrug Micellar Nanoparticles as a Versatile and Potent Platform for Cancer Therapy. *Biomacromolecules* **2013**, *14*, 2772−2780.
(33) Hershberger, K. K.; Gauger, A. J.; Bronstein, L. M. Utilizing Stimuli Responsive Linkages to Engineer and Enhance Polymer Nanoparticle-Based Drug Delivery Platforms. *ACS Appl. Bio Mater.* **2021**, *4*, 4720−4736.
(34) Yuvaraj, A.; Ghosh, R.; Domb, A. J. Biodegradable Hydrophobic Injectable Polymers for Drug Delivery and Regenerative Medicine. *Adv. Funct. Mater.* **2021**, *31*, 2010284.
(35) Pramod, P. S.; Takamura, K.; Chaphekar, S.; Balasubramanian, N.; Jayakannan, M. Dextran Vesicular Carriers for Dual Encapsulation of Hydrophilic and Hydrophobic Molecules and Delivery into Cells. *Biomacromolecules* **2012**, *13*, 3627−3640.
(36) Anas, M.; Jana, S.; Mandal, T. K. Vesicular assemblies of thermoresponsive amphiphilic polypeptide copolymers for guest encapsulation and release. *Polym. Chem.* **2020**, *11*, 2889−2903.
(37) Balachandran, V. S.; Jadhav, S. R.; Vemula, P. K.; John, G. Recent Advances in Cardanol Chemistry in a Nutshell: From a Nut to Nanomaterials. *Chem. Soc. Rev.* **2013**, *42*, 427−438.
(38) Pramod, P. S.; Shah, R.; Jayakannan, M. Dual Stimuli Polysaccharide Nanovesicle for Conjugated and Physically Loaded Doxorubicin delivery in Breast Cancer Cells. *Nanoscale* **2015**, *7*, 6636−6652.
(39) Inchanalkar, S.; Deshpande, N. U.; Kasherwal, V.; Jayakannan, M.; Balasubramanian, N. Polymer Nanovesicle Mediated Delivery of MLN8237 Preferentially inhibits Aurora Kinase A to target RalA and Anchorage-Independent Growth in Breast Cancer Cells. *Mol. Pharmaceutics* **2018**, *15*, 3046−3059.
(40) Deshpande, N. U.; Jayakannan, M. Biotin-Tagged Polysaccharide Vesicular Nanocarriers for Receptor- Mediated Anticancer Drug Delivery in Cancer Cells. *Biomacromolecules* **2018**, *19*, 3572−3585.
(41) Deshpande, N. U.; Jayakannan, M. Cisplatin-Stitched Polysaccharide Vesicles for Synergistic Cancer Therapy of Triple Antagonistic Drugs. *Biomacromolecules* **2017**, *18*, 113−126.
(42) Pramod, P. S.; Shah, R.; Chaphekar, S.; Balasubramanian, N.; Jayakannan, M. Polysaccharide Nano-Vesicular Multidrug Carriers for Synergistic Killing of Cancer Cells. *Nanoscale* **2014**, *6*, 11841−11855.
(43) Pramod, P. S.; Deshpande, N. U.; Jayakannan, M. Real-Time Drug Release Analysis of Enzyme and pH Responsive Polysaccharide Nanovesicles. *J. Phys. Chem. B* **2015**, *119*, 10511−10523.
(44) Zhang, N.; Chen, H.; Fan, Y.; Zhou, L.; Trépout, S.; Guo, J.; Li, M.-H. Fluorescent Polymersomes with Aggregation-Induced Emission. *ACS Nano* **2018**, *12*, 4025−4035.
(45) Zhang, D.; Fan, Y.; Chen, H.; Trépout, S.; Li, M.-H. $CO_2$-Activated Reversible Transition between Polymersomes and Micelles with AIE Fluorescence. *Angew. Chem., Int. Ed.* **2019**, *58*, 10260−10265.
(46) Deshpande, N. U.; Virmani, M.; Jayakannan, M. An AIE-driven Fluorescent Polysaccharide Polymersome as an Enzyme-Responsive FRET Nanoprobe to Study the Real-Time Delivery Aspects in Live Cells. *Polym. Chem.* **2021**, *12*, 1549−1561.
(47) Kashyap, S.; Jayakannan, M. Amphiphilic Diblocks Sorting into Multivesicular Bodies and Their Fluorophore Encapsulation Capabilities. *J. Phys. Chem. B* **2012**, *116*, 9820−9831.
(48) Ringsdorf, H.; Schlarb, B.; Venzmer, J. Molecular Architectures and Function of Polymeric Oriented Systems: Models for the Study of Organization, Surface Recognition, and Dynamics of Biomembranes. *Angew. Chem., Int. Ed.* **1998**, *27*, 113−138.
(49) Xue, X.; Zhao, Y.; Dai, L.; Zhang, X.; Hao, X.; Zhang, C.; Huo, S.; Liu, J.; Liu, C.; Kumar, A.; Chen, W.-Q.; Zou, G.; Liang, X.-J. Spatiotemporal Drug Release Visualized through a Drug Delivery System with Tunable Aggregation-Induced Emission. *Adv. Mater.* **2014**, *26*, 712−717.
(50) Xue, X.; Jin, S.; Zhang, C.; Yang, K.; Huo, S.; Chen, F.; Zou, G.; Liang, X.-J. Probe-Inspired Nano-Prodrug with Dual-Color Fluorogenic Property Reveals Spatiotemporal Drug Release in Living Cells. *ACS Nano* **2015**, *9*, 2729−2739.
(51) Yuan, Y.; Kwok, R. T. K.; Zhang, R.; Tang, B. Z.; Liu, B. Targeted Theranostic Prodrugs Based on an Aggregation-Induced Emission (AIE) Luminogen for Real-Time Dual-Drug Tracking. *Chem. Commun.* **2014**, *50*, 11465−11468.
(52) Yuan, Y.; Chen, Y.; Tang, B. Z.; Liu, B. A Targeted Theranostic Platinum(iv) Prodrug Containing a Luminogen with Aggregation-Induced Emission (AIE) Characteristics for in Situ Monitoring of Drug Activation. *Chem. Commun.* **2014**, *50*, 3868−3870.
(53) Gao, X.; Cao, J.; Song, Y.; Shu, X.; Liu, J.; Sun, J. Z.; Liu, B.; Tang, B. Z. A Unimolecular Theranostic System with H2O2-Specific Response and AIE-activity for Doxorubicin releasing and Real-time Tracking in Living Cells. *RSC Adv.* **2018**, *8*, 10975−10979.
(54) Torres, M.; Khan, S.; Duplanty, M.; Lozano, H. C.; Morris, T. J.; Nguyen, T.; Rostovtsev, Y. V.; DeYonker, N. J.; Mirsaleh-Kohan, N. Raman and Infrared Studies of Platinum-Based Drugs: Cisplatin, Carboplatin, Oxaliplatin, Nedaplatin, and Heptaplatin. *J. Phys. Chem. A* **2018**, *122*, 6934−6952.
(55) Surnar, B.; Sharma, K.; Jayakannan, M. Core−shell polymer nanoparticles for prevention of GSH drug detoxification and cisplatin delivery to breast cancer cells. *Nanoscale* **2015**, *7*, 17964−17979.


https://doi.org/10.1021/acspolymersau.1c00042
*ACS Polym. Au* 2022, 2, 181−193